


Collagen fibers quantification for liver fibrosis assessment using linear dichroism photoacoustic microscopy

Yang Qiu ^{a,1}, Honghui Li ^{a,1}, Kun Yu ^{a,b}, Jiali Chen ^{a,b}, Li Qi ^c, Yinghua Zhao ^{d,*},
Liming Nie ^{a,*} 

^a Optical Molecular Imaging Laboratory, Medical Research Institute, Guangdong Provincial People's Hospital (Guangdong Academy of Medical Sciences), Southern Medical University, Guangzhou 510080, China

^b School of Medicine, South China University of Technology, Guangzhou 510006, China

^c School of Biomedical Engineering, Southern Medical University, Guangzhou 510900, China

^d Department of Medical Imaging, Third Affiliated Hospital of Southern Medical University (Academy of Orthopedics Guangdong Province), Southern Medical University, Guangzhou 510630, China

ARTICLE INFO

Keywords:

Liver fibrosis
Collagen fibers
Linear dichroism
Photoacoustic imaging

ABSTRACT

Liver fibrosis represents a progressive pathological condition that can culminate in severe hepatic dysfunction, potentially advancing to cirrhosis and liver cancer. The extent of liver fibrosis is intrinsically associated with the quantity of collagen fibers. Although liver biopsy and ultrasound imaging are standard diagnostic tools, their application is constrained by risks of significant complications and variability in different investigators, respectively. In this study, we utilized linear dichroism photoacoustic microscopy (LDPAM) to visualize and quantify collagen fibers, which exhibit specific absorption of polarized light, subsequently calculating a collagen fibers degree of dichroism (CDOD) score. We obtained high-resolution images of liver structures, with an emphasis on collagen fibers within the hepatic tissue. Using the CDOD score, we categorized liver fibrosis into three distinct stages: normal, early, and advanced. For validation purposes, collagen fibers were visualized with Sirius-red staining and quantitatively assessed through the collagen proportional area (CPA) score. Our results demonstrated a significant correlation between the CDOD and CPA scores, with a Pearson coefficient of 0.95. This approach presents a promising and non-invasive method for assessing liver fibrosis by quantifying collagen fibers.

1. Introduction

Liver fibrosis is a prevalent pathological feature in liver diseases, where the severity of fibrosis is closely associated with the accumulation of collagen fibers [1]. This progression is acknowledged as dynamic and potentially reversible with timely intervention targeting the underlying cause and effective therapies [2]. Therefore, early and precise evaluation of liver fibrosis is crucial in clinical settings for devising appropriate treatment strategies and predicting outcomes. Although liver biopsy is widely recognized as the gold standard for diagnosing and staging liver fibrosis [3]. However, the invasiveness of repeated biopsies over a short period presents practical constraints and potential complications, hindering the clinical utility of monitoring disease progression dynamically [4,5].

Qualitative and quantitative imaging modalities have been integrated into ultrasound and MRI to stage liver fibrosis as alternatives to liver biopsy [6,7]. Ultrasound elastography techniques provide non-invasive means of diagnosing liver fibrosis. Nonetheless, vibration controlled transient elastography is hindered by ambiguous cutoff values and reliance on operator skill [8]. Point shear wave elastography demonstrates superior diagnostic accuracy and is less influenced by obesity, although it is limited by a smaller area of assessment [9]. Two-dimensional shear wave elastography provides measurements across larger tissue areas but lacks comprehensive validation [10]. Additionally, magnetic resonance imaging-based elastography is a diagnostic technique utilized for assessing of liver fibrosis [11]. This method employs existing MRI scanners to assess liver stiffness by generating shear waves through acoustic vibrations. While offering a

* Corresponding authors.

E-mail addresses: zyh7258957@163.com (Y. Zhao), limingnie@gmail.com (L. Nie).

¹ These authors contributed equally to this work.

thorough evaluation of liver health with a high level of reproducibility [12], technical difficulties may be encountered in certain scenarios, such as cases involving iron overload or ascites [13]. These techniques contribute to the assessment of liver fibrosis, each with its own limitations.

Photoacoustic microscopy (PAM) has gained prominence as an emerging biomedical imaging technique [14], demonstrating promise in the detection and evaluation of liver pathologies owing to its high resolution and non-invasive [15]. PAM utilizes the photoacoustic effect to acquire comprehensive structural and functional information from tissues by detecting acoustic signals generated from light absorption within the tissues [16]. Nevertheless, conventional PAM predominantly depends on the disparate absorption coefficients of different tissue components to provide contrast. This approach disregards the dichroism exhibited by collagen fibers, which exhibit varying absorption coefficients under different angles of polarized light [17,18]. This omission poses a significant obstacle in achieving accurate imaging, particularly in the presence of substantial blood absorption interference [19].

Given these limitations, this study presents a liver fibrosis diagnostic method using a linear dichroism photoacoustic microscopy (LDPAM) system as shown in Fig. 1. In contrast to conventional PAM techniques, we modulate the excitation light into polarized light with adjustable orientation [20]. By capturing photoacoustic images from multiple angles of polarized light, we can generate collagen fiber degree of dichroism (CDOD) images that illustrate the extent of collagen fibers deposition for assessing liver fibrosis. This approach has the potential to improve the assessment of liver pathology during surgical procedures, assisting in making informed decisions regarding tissue resection to preserve healthy areas.

2. Material and methods

2.1. Principle of linear dichroism photoacoustic microscopy

In conventional photoacoustic imaging, the initial pressure p is expressed as

$$p = \Gamma \eta_{th} \mu_a F \quad (1)$$

Where Γ is the Grueneisen parameter, η_{th} is the thermal conversion efficiency, μ_a represents optical absorption coefficient, and F represents optical fluence [21]. We further investigate the polarization properties

of the scanned samples and the excitation laser, specifically by considering the dichroism and polarization angles. The μ_a was changed with laser polarization angle φ , assume the sample optical axis orientation is θ , the μ_a is expressed as

$$\begin{aligned} \mu_a(\varphi, \theta) &= \mu_p \cos^2(\theta - \varphi) + \mu_v \sin^2(\theta - \varphi) \\ &= \frac{\mu_p + \mu_v}{2} + \frac{\mu_p - \mu_v}{2} \cos(2\varphi - 2\theta) \end{aligned} \quad (2)$$

Where μ_p and μ_v represents optical absorption coefficient while laser polarization orientation parallel and vertical to the sample optical axis orientation [19]. Using LDPAM to image the dichroism sample, initial pressure $p(\theta, \varphi)$ can be expressed as

$$p(\varphi, \theta) = \Gamma \eta_{th} \left[\frac{\mu_p + \mu_v}{2} + \frac{\mu_p - \mu_v}{2} \cos(2\varphi - 2\theta) \right] F \quad (3)$$

It can be know the PA signal changes with laser polarization orientation present the form of a sinus function, to imagine the dichroism degree of the sample, we measure PA signal amplitude excited by four polarization orientations of $p(0^\circ, \theta)$, $p(45^\circ, \theta)$, $p(90^\circ, \theta)$, and $p(-45^\circ, \theta)$ respectively. Defined the degree of dichroism (DOD) of sample as

$$DOD = \sqrt{Q_{PA}^2 + U_{PA}^2} / I_{PA} \quad (4)$$

Where $Q_{PA} = p(0^\circ, \theta) - p(90^\circ, \theta)$, $U_{PA} = p(45^\circ, \theta) - p(-45^\circ, \theta)$, $I_{PA} = p(0^\circ, \theta) + p(90^\circ, \theta)$. Therefore, LDPAM system can quantify the degree of dichroism of the sample.

2.2. System setup

Fig. 2 illustrates the schematic of the LDPAM system, which utilizes a 532-nm pulsed laser (FOTIA 532, Inno-laser) with a pulse width of 5 ns and a repetition frequency of 5 kHz as the excitation source. During imaging, the laser power was set to 1.25 mW, and the energy per pulse was calculated as 250 nJ. The laser output is first spatially filtered through a pinhole, then split into two paths using a polarization beam splitter cube. One path is directed towards a photodiode (PDA10A2 - Si Fixed Gain Detector, Thorlabs) to monitor changes in laser intensity, while the other path is transmitted through polarizer 1 to achieve full linear polarization of the laser beam. Following this, the laser beam undergoes polarization manipulation by passing through a $\lambda/4$ plate to

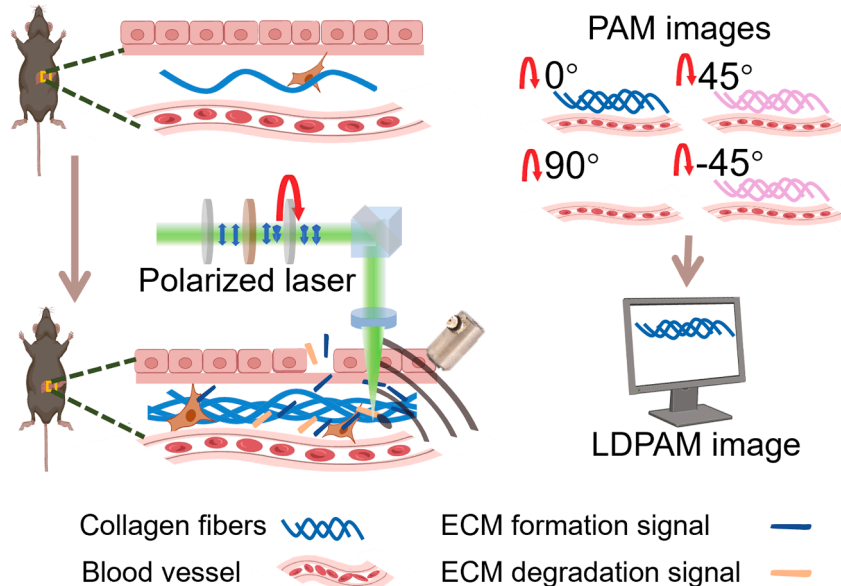


Fig. 1. Schematic of the linear dichroism photoacoustic microscopy system quantifying collagen fibers.

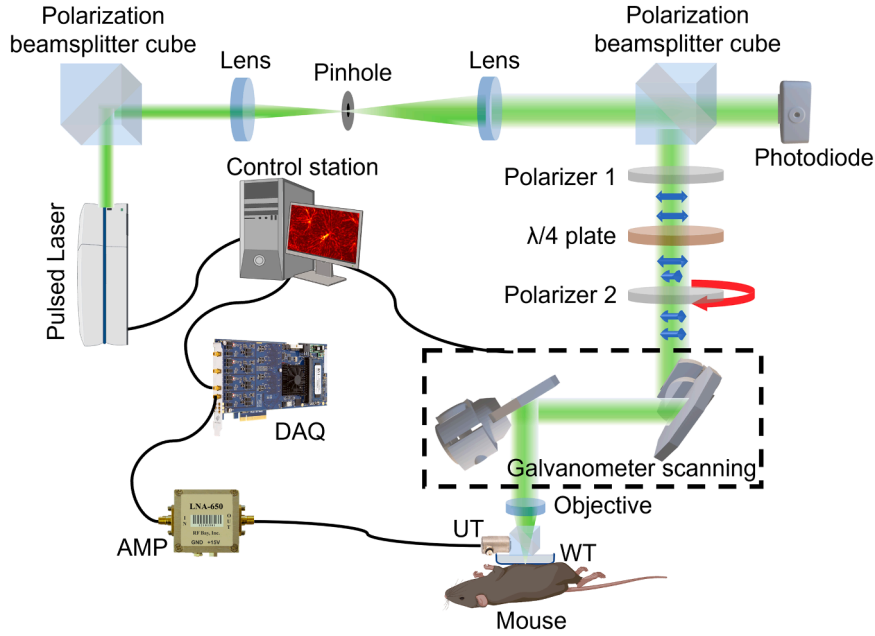


Fig. 2. Schematic of the linear dichroism photoacoustic microscopy system. DAQ, digitizer acquisition; AMP, amplifier; UT, ultrasound transducer; WT, water tank.

achieve circular polarization, then through polarizer 2 to achieve linear polarization with varying orientations achieved by rotating polarizer 2 [22]. The polarized laser beam is directed through a galvanometer scanning system to enable single pulse laser excitation of the sample in a point-by-point manner is focused onto the sample using achromatic lenses (AC127-050-AB - $f = 50.0$ mm, $\text{Ø}1/2''$, Thorlabs). The photoacoustic effect generates ultrasound waves that are amplified by an amplifier (LNA-650, RF BAY) and received by an ultrasonic transducer (V214-BC-RM, Olympus), then converted into PA signals by a digitizer acquisition card (M4i.4420-x8, Spectrum-instrumentation).

2.3. Phantom experiment

To validate the LDPAM for dichroism sample imaging, we conducted a phantom experiment by placing a polarizer on the left side and a piece of black tape on the right side, with a small gap between them, as shown in Fig. 3(a). The polarizer exhibits stronger dichroism compared to the black tape. We imaged the phantom using the LDPAM system with different polarization orientations of the laser to obtain sequential images, with an imaging area of $0.9 \text{ mm} \times 0.9 \text{ mm}$ and a single scan time of 12 seconds. Subsequently, we extracted the variation curve of PA signal amplitude with polarization orientation and calculated the DOD to compare the degree of dichroism. To assess the impact of blood absorption on the penetration depth, linearly polarized light passed through diluted bovine blood phantoms (1:5 dilution with PBS) at varying thicknesses (Fig. 3(f)).

To further image tissues in the presence of blood absorption, we made a phantom composed of bovine achilles tissue and blood as shown in Fig. 3(i). The transmitted light intensity was measured at different polarization angles using a photodiode, and the degree of linear polarization (DLP) was calculated to analyze the effect of blood phantom thickness on the polarization state. The DLP was calculated using the formula:

$$DLP = \frac{\sqrt{(I_H - I_V)^2 + (I_P - I_M)^2}}{I_H + I_V} \quad (5)$$

Where I_H, I_V, I_P and I_M correspond to the light intensities at polarizer orientations of $0^\circ, 90^\circ, 45^\circ$, and -45° , respectively.

2.4. Disease models

All animal experiments were performed in compliance with the Guidelines for the Care and Use of Research Animals established by the Institutional Ethical Committee of Animal Experimentation of Guangdong Provincial People's Hospital (KY2024-095-01) in China. Experiments were carried out on 18 healthy male C57BL/6 mice aged 6 weeks and weighing 16–18 g, sourced from the Guangdong Medical Laboratory Animal Center. The mice were kept in controlled conditions at a temperature of $24 \pm 2^\circ \text{C}$, a 12-hour light/dark cycle, and relative humidity maintained at $50 \pm 5\%$ [23]. To mimic the progression of liver fibrosis, a 20% carbon tetrachloride solution (56-23-5, Macklin) prepared in olive oil was injected into the abdominal cavity of the mice at a dose of 2 ml/kg [24]. The injection protocol was administered three times a week on Mondays, Wednesdays, and Fridays for ten weeks.

2.5. LDPAM imaging of in vitro experiments

We conducted an in vitro experiment to verify the capability of the LDPAM system to specifically image collagen fibers. Subsequently, two consecutive slices were obtained from the fixed liver tissue: one slice underwent Sirius-red staining and was examined under a microscope to assess collagen fiber structure as a control, while the other slice was imaged with the LDPAM system, and the CDOD image was calculated using (4) to correlate with the Sirius-red staining results.

2.6. LDPAM imaging of liver

The LDPAM system was used for liver imaging in both control mice and mice with induced liver fibrosis over a period of 10 weeks. Anesthesia was induced with 2% isoflurane [25], and abdominal hair was removed prior to incising the skin for liver exposure during imaging. A point-by-point scan was conducted using a pulsed laser with a power of 1.25 mW [15], a repetition rate of 5 kHz, and a scan duration of 12 seconds. Imaging of the same area was performed with four different laser polarization orientations: $0^\circ, 90^\circ, 45^\circ$, and -45° . The maximum amplitude projection was used to obtain photoacoustic images. Each scan took 12 seconds, and the total scan time did not exceed 60 seconds. The scanning range was $0.9 \text{ mm} \times 0.9 \text{ mm}$ in the horizontal plane, with an imaging depth of $1536 \mu\text{m}$ in the vertical direction. Photoacoustic

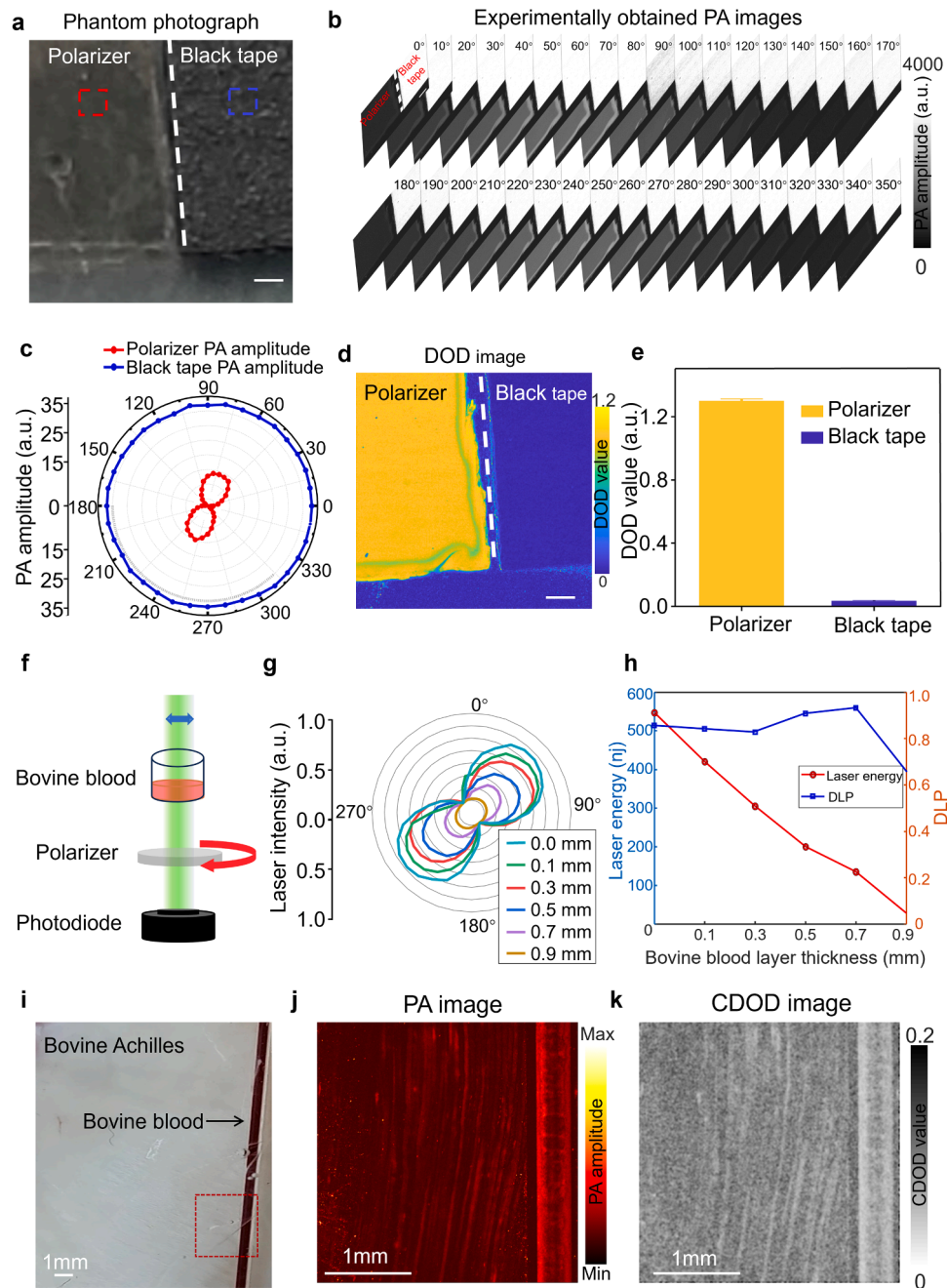


Fig. 3. Quantitative LDPAM imaging of the phantom. (a) Photograph of the phantom, the phantom consists of a polarizer and black tape, located on the left and right respectively. (b) A sequence of PA images acquired by rotating polarizer 36 times with the step of 10 degrees. (c) The quantitative results of PA signal amplitude in (b) of ROI region in (a). (d) DOD image of the phantom. (e) Quantitative results of DOD value comparison of polarizer and black tape in (d). (f) Schematic diagram of the experimental setup for testing polarization modulation through bovine blood. (g) Polarization diagram showing the transmitted light intensity as a function of the polarizer angle for different blood thicknesses. (h) Degree of linear polarization (DLP) as a function of blood thickness. (i) Experimental setup for imaging a combined tissue phantom consisting of bovine achilles tissue and blood. (j) PA image of the phantom in (i). (k) CDOD image of the phantom in (i). Scale bar = 100 μm .

images obtained from different excitation laser polarization orientations were analyzed to compute the CDOD image. A threshold for CDOD was set to identify regions with collagen fibers in the livers of control mice. The mean CDOD values of regions exceeding this threshold were calculated to quantify collagen fiber content.

2.7. Liver biopsy and histopathologic evaluation

A liver biopsy was performed after imaging, liver samples from the mice were fixed in 4 % buffered formalin [26]. After fixation, the tissues were dehydrated in alcohol, cleared in xylene, and then embedded in

paraffin. The samples were then sliced into 5- μm thick sections and stained with hematoxylin and eosin (H&E) to comprehensively examine the liver tissues. Additionally, Sirius-red staining was used to visualize collagen deposition in the liver tissue [27]. The slices were then examined and photographed under a light microscope.

2.8. Image analysis

The LDPAM images were analyzed and quantified using a custom-written MATLAB R2022b program (MathWorks, Inc.). The raw data from each scan initially formed a three-dimensional matrix, where each

voxel's value represented the photoacoustic signal intensity in the 3D space. The data were then transformed into a two-dimensional maximum amplitude projections (MAP) image. Before calculating the CDOD, image registration was conducted to correct for potential small positional discrepancies in the MAP images due to different excitation laser polarization orientations. This registration process involved aligning the four images to ensure accurate comparison and analysis. Feature points were extracted from each image and matched to establish correspondences. Then a transformation model involving translation and rotation was selected to describe the spatial relationship between the images. The optimization process aimed to minimize the mean squared error as the error metric by iteratively adjusting the transformation parameters. This iterative process continued until convergence was achieved, ensuring optimal alignment among the images. By using this registration method, precise spatial alignment was achieved, enhancing the reliability of subsequent analyses. The registered images were then substituted into (4) to calculate the CDOD image, followed by generating a grayscale histogram to calculate the CDOD score.

Additionally, our proprietary MATLAB code was used for quantitative analysis of the pathologically stained images. Using an adaptive thresholding technique, the stained images were binarized to extract the collagen fiber structure, and the area percentage was calculated to obtain the collagen proportional area (CPA) score.

2.9. Statistical analysis

The statistical analysis was performed using SPSS for Windows (version 26, IBM), to assess the accuracy of the CDOD score in diagnosing liver fibrosis, with CPA score as the gold standard. Descriptive statistics were used to summarize the distribution of CDOD and CPA score, including metrics like minimum, first quartile, median, third quartile. One-way analysis of variance (ANOVA) was conducted to compare CDOD score at different modeling times [28]. Additionally, the Pearson correlation coefficient was used to evaluate the correlation between CDOD and CPA scores, based on the data distribution. A receiver operating characteristic (ROC) curve was generated to evaluate the diagnostic performance of the CDOD score in predicting liver fibrosis compared to the CPA score. Then, the area under the curve (AUC) was calculated to quantify the diagnostic capability. Statistical significance was set at $p < 0.05$. Results were interpreted in accordance with the study's objectives.

3. Results

3.1. Quantitative LDPAM imaging of the phantom and liver slice

The outcomes of the phantom experiment are illustrated in Fig. 3. Fig. 3(a) presents a photograph of the phantom, which includes a polarizer and black tape positioned on the left and right sides, respectively. The polarizer exhibits pronounced dichroism in contrast to the black tape. Fig. 3(b) shows 36 photoacoustic (PA) images acquired by rotating the polarizer through 36 different polarized laser excitations. The PA signal amplitude of the polarizer displays periodic variations, whereas the PA signal amplitude of the black tape remains relatively constant. Fig. 3(c) presents the quantitative analysis of the PA signal amplitude for both the polarizer and black tape within the region of interest (ROI) delineated in Fig. 3(a). Furthermore, Figs. 3(d) and 3(e) display the degree of dichroism derived from the PA images. The mean DOD value for the polarizer is 1.3007, whereas for the black tape, it is 0.0341. These findings demonstrate that LDPAM imaging can effectively distinguish between dichroic and non-dichroic samples. Fig. 3(g) illustrates the relationship between transmitted laser intensities penetrating blood layers at various thicknesses and excited polarizer angles. Fig. 3(h) depicts the changes in both laser energy and DLP relative to penetration depth. As the thickness of the bovine blood layer increased, the transmitted light intensity decreased. Nonetheless, the DLP remained

almost constant when the thickness of bovine blood layer reached ≤ 0.7 mm, indicating that the polarization state of the light was not influenced by blood absorption at shallow depth. In Fig. 3(j), bovine blood demonstrated a strong absorption signal, whereas the bovine achilles tendon, rich in collagen fibers, exhibited a much weaker signal. Despite the significant absorption by the blood, the CDOD image in Fig. 3(k) revealed that the collagen fibers in the bovine achilles tissue were still detectable. This result confirms that LDPAM can effectively image collagen fibers, even in the presence of a strong blood background.

To further validate the imaging capability of the LDPAM system for collagen fibers in liver tissue, we conducted experiments on two consecutive slices of mouse liver tissue, as illustrated in Fig. 4. Figs. 4(a) and 4(b) depict the stained and unstained slices, respectively. Fig. 4(a) presents the outcome of Sirius-red staining, with the corresponding microscope scan shown in Fig. 4(d). Conversely, Fig. 4(b) was imaged using LDPAM, with the results displayed in Fig. 4(c). The area indicated by the arrow highlights a cross-section of a blood vessel exhibiting a strong signal attributable to the presence of blood. The CDOD results presented in Fig. 4(e) indicate a low CDOD value (< 0.0582) within the blood vessel area, as denoted by the red arrow, whereas the collagen fibers on the blood vessel wall exhibit a high CDOD value (> 0.1169). Fig. 4(f), which represents the overlay of Figs. 4(d) and 4(e), corroborates the presence of collagen fibers. These findings demonstrate that LDPAM imaging can effectively and specifically identify collagen fibers.

3.2. In vivo LDPAM imaging of liver

To determine the threshold of CDOD, we imaged the control group, which included control-M1, control-M2, and control-M3. The PA images of M1, M2, and M3 are shown in Figs. 5(a), 5(d), and 5(g), respectively. The corresponding CDOD images are displayed in Figs. 5(b), 5(e), and 5(h). As the normal mouse liver also contains collagen fibers, with a CPA of less than 4.8% [5,29], we counted the CDOD values in the CDOD images from small to large and plotted them into histograms. The CDOD value at 95.2% was selected as the threshold. The CDOD thresholds for M1, M2, and M3 were determined to be 0.1233, 0.1164, and 0.1246, respectively. Finally, the average CDOD threshold of the control group 0.1214 was taken as the threshold for collagen fibers.

After determining the CDOD threshold for collagen fibers, we used this threshold to quantify the severity of liver fibrosis in model mice. Fig. 6 shows the results of liver imaging by the LDPAM system at different modeling times. The PA images of control and model mice at 2 weeks, 4 weeks, 6 weeks, 8 weeks, and 10 weeks are displayed in Fig. 6(a). Due to the liver containing a large amount of blood for in vivo imaging, and blood having strong absorption of the 532 nm pulsed laser [30], the PA images can clearly visualize the blood vessel structure but cannot directly reflect the content of collagen fibers in the imaging area [31]. The CDOD images were calculated using PA images with different excitation laser polarization orientations, as shown in Fig. 6(b). The contrast in the CDOD image arises from dichroism, removing the blood vessel structure and enabling reflection of the content of collagen fibers. To quantify collagen fibers, the CDOD score was statistically calculated using the threshold determined by the control group and defined as the average value of the CDOD values greater than the threshold. The CDOD score at different modeling times was calculated with only typical presented in Figs. 6(c) to 6(h).

3.3. Liver histopathologic analysis

Fig. 7(a) depicts photographs of the livers of mice in vivo at different modeling times. During the progression of liver fibrosis, the edges of the liver undergo changes characterized by irregularity and loss of smoothness. Fig. 7(b) displays the histological results of Hematoxylin and Eosin staining, Sirius-red staining, and collagen fiber extraction in the control group. In contrast, Figs. 7(c) to 7(g) present the results of 2

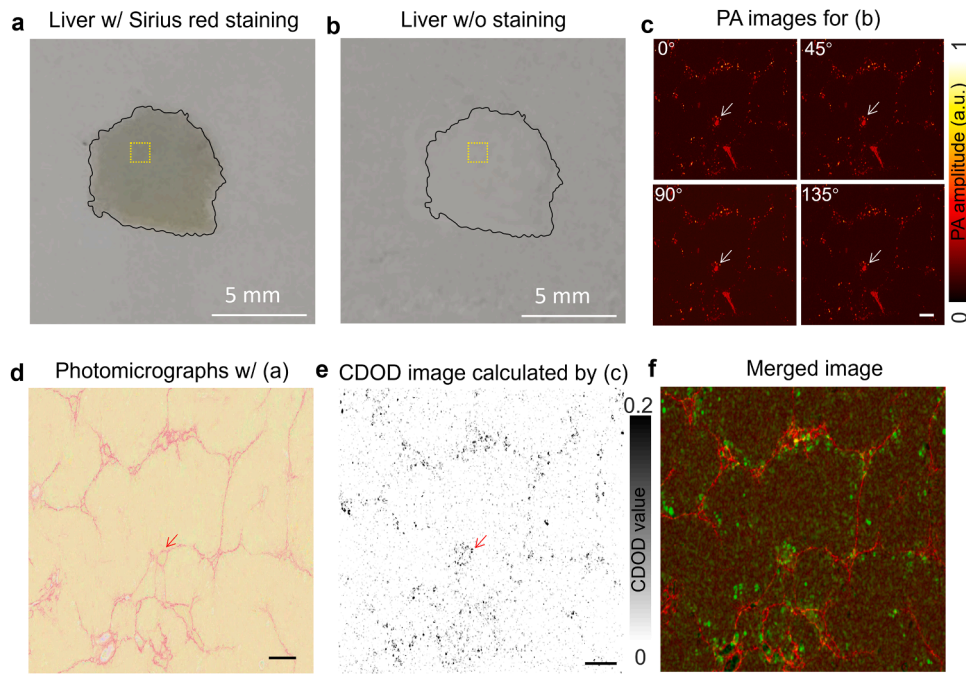


Fig. 4. LDPAM imaging of liver slices. (a) Sirius-red staining results of the liver slice in liver fibrosis group. (b) The photograph of mouse liver slice without stained. (c) PA images of (b) acquired by LDPAM system with four polarization angles representative. (d) Microscope scan results of the liver area in (a). (e) CDOD image calculated by (c). (f) Results of merging images in panels (d) and (e). Scale bar = 100 μm .

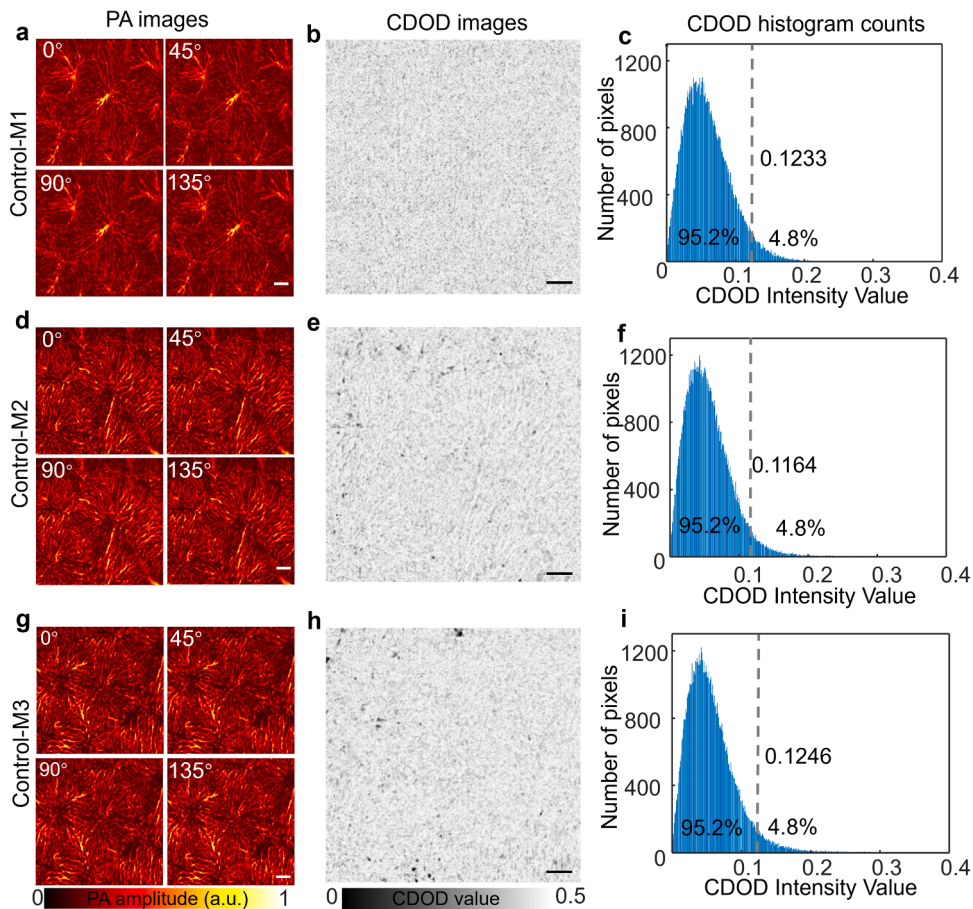


Fig. 5. In vivo LDPAM imaging of liver in normal group. (a) PA images of M1, M2 (d) and M3 (g) in normal group. (b) CDOD images of M1, M2 (e) and M3 (h) in normal group. (c) CDOD histogram counts of M1, M2 (f) and M3 (i) in normal group. Scale bar = 100 μm .

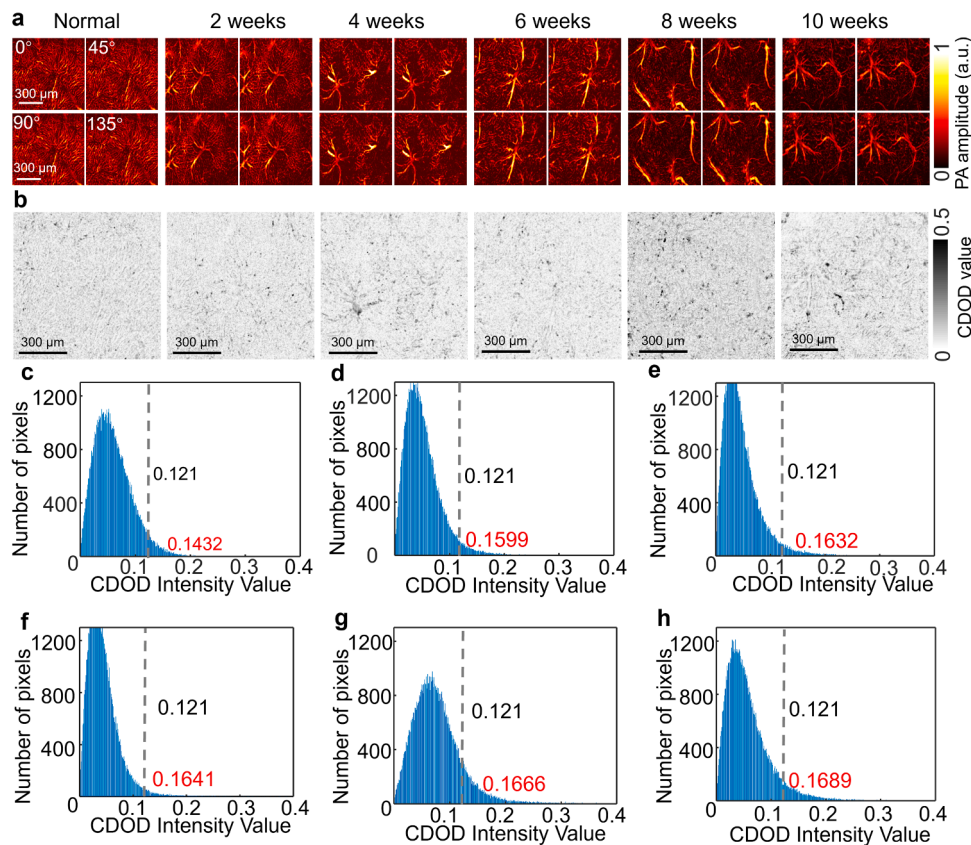


Fig. 6. In vivo LDPAM imaging of the liver in normal and liver fibrosis groups. (a) LDPAM images acquired by different polarization angles of normal and fibrosis groups. (b) CDOD images of normal and fibrosis groups. (c) CDOD histogram counts of normal group, 2 weeks (d), 4 weeks (e), 6 weeks (f), 8 weeks (g) and 10 weeks (h).

weeks, 4 weeks, 6 weeks, 8 weeks, and 10 weeks. The collagen proportional area (CPA) score was defined as the percentage of the area positive for collagen fiber extraction, and we quantified collagen fibers by calculating the CPA score (control group, 0.1492 ± 0.0056 ; 2 weeks, 4.8228 ± 0.3009 ; 4 weeks, 5.3894 ± 0.1928 ; 6 weeks, 6.2592 ± 0.4054 ; 8 weeks, 7.6086 ± 0.5424 ; 10 weeks, 9.3968 ± 0.8650 ; $p < 0.001$). Based on the H&E and Sirius-red staining results obtained from different modeling times, progressive changes indicative of fibrosis can be observed. The H&E staining across varying modeling periods reveals consistent alterations in liver tissue morphology, including increased nuclear density, disrupted cell alignment, and distortion of hepatic lobular structure. In parallel, the Sirius-red staining demonstrates a time-dependent escalation in collagen fibers deposition within the liver tissue reflecting advancing fibrotic processes. These combined findings underscore the evolving nature of fibrosis over different modeling periods, highlighting the temporal dynamics of collagen accumulation in the liver tissue.

3.4. Quantitative analysis of LDPAM results and correlation analysis with Sirius-red staining results

To quantitatively evaluate the performance of the LDPAM system in diagnosing liver fibrosis, we summarized the box plots from quantitative analysis of CDOD and CPA scores and performed a correlation analysis between the CDOD score and the pathological CPA score. Additionally, we conducted ROC analysis to evaluate the effectiveness of the LDPAM system in discriminating different stages of fibrosis.

Fig. 8(a) illustrates the results of the CDOD score in different stages of fibrosis (control group, 0.1495 ± 0.0056 ; 2 weeks, 0.1589 ± 0.0011 ; 4 weeks, 0.1621 ± 0.0011 ; 6 weeks, 0.1632 ± 0.0009 ; 8 weeks, 0.1671 ± 0.0022 ; 10 weeks, 0.1700 ± 0.0016 ; $p < 0.001$). Fig. 8(b) illustrates

the results of the CPA score, with the lowest CPA score in the 2 weeks results being 4.47 %, and the smallest CPA score in the 10 weeks results being 8.52 %. We considered 4.47 % to be the boundary value between normal and early fibrosis, and 8.52 % to be the boundary value between early and advanced fibrosis. All mice were separated based on their CPA score into three categories: no fibrosis (CPA score ≤ 4.47 %), early fibrosis (CPA score 4.47–8.52 %), and advanced fibrosis (CPA score > 8.52 %). We then performed ROC analysis to evaluate the effectiveness of the CDOD score in discriminating different stages of fibrosis determined by the CPA score. Fig. 8(c) shows that the AUC for distinguishing fibrotic (CPA score > 4.47 %) from nonfibrotic (CPA ≤ 4.47 %) livers was 1, indicating perfect discrimination. The 95 % confidence interval (CI) for this AUC, calculated using bootstrapping with 1000 resamples, ranged from 1.0000 to 1.0000. Similarly, Fig. 8(d) shows that the AUC for distinguishing advanced fibrosis (CPA score > 8.52 %) livers was 0.9815, indicating high discriminatory power. The 95 % CI for this AUC ranged from 0.9735 to 0.9895. Furthermore, we found a significant correlation between the CPA and CDOD scores, as shown in Fig. 8(e), with a coefficient of 0.95 ($R^2 = 0.91$). This strong correlation underscores the reliability and validity of the LDPAM system in assessing liver fibrosis.

4. Discussion

This study presents LDPAM, an innovative diagnostic tool for liver fibrosis, which facilitates continuous, non-invasive monitoring with enhanced resolution. By modulating the excitation laser polarization, LDPAM quantitatively evaluates the accumulation of collagen fibers in liver tissue, thereby providing critical insights into the progression of fibrosis.

Through the quantification of collagen fibers and their correlation

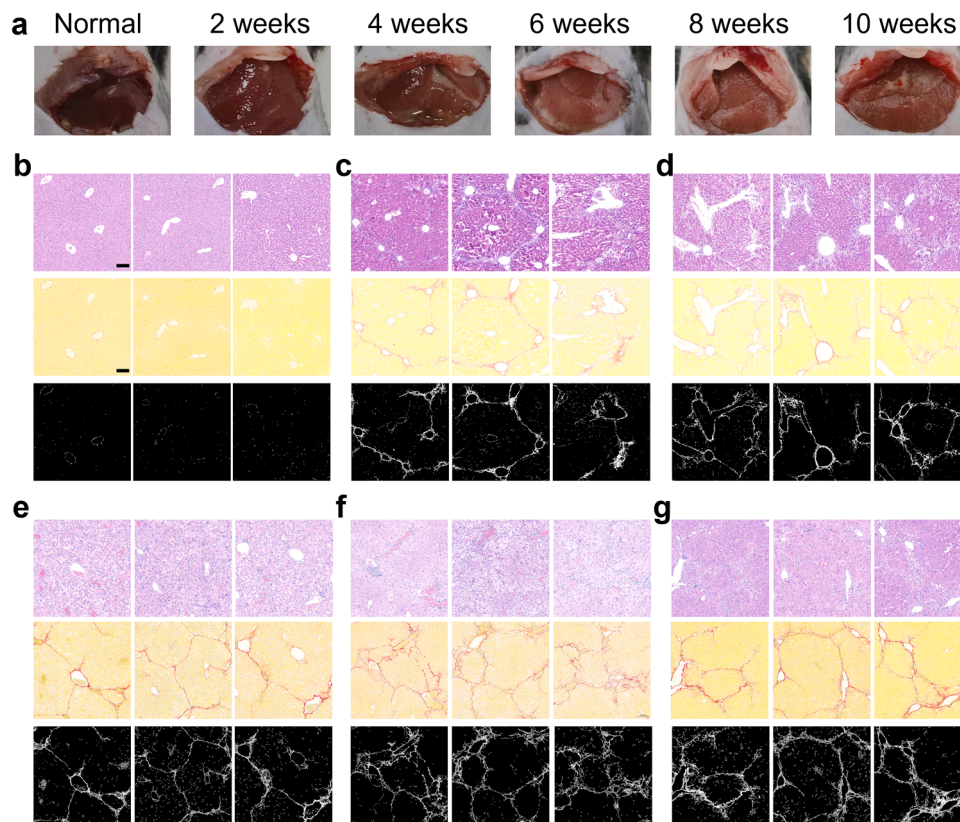


Fig. 7. Liver histopathologic analysis of normal and modeling mice at different stages. (a) Photographs of the liver at different stages. (b) Results of Hematoxylin Eosin (the first line), Sirius-red staining (the second line) and collagen fibers extraction (the third line) in normal group. (c) Results of H&E, Sirius-red staining and collagen fibers extraction in liver fibrosis 2 weeks (c), 4 weeks (d), 6 weeks (e), 8 weeks (f), 10 weeks (g) groups. Scale bar = 100 μm .

with histopathological findings, we established thresholds to differentiate between normal, early fibrosis, and advanced fibrosis stages. This approach improves the accuracy and reliability of fibrosis diagnosis, potentially minimizing the necessity for invasive liver biopsies. Our findings demonstrate a strong correlation between the CDOD score derived from LDPAM imaging and the CPA score obtained from histological analysis. Furthermore, the high sensitivity and specificity of LDPAM, as confirmed by ROC analysis, underscore its potential as a liver fibrosis staging tool. This method is instrumental for monitoring disease progression and assessing treatment efficacy, rendering it ideal for long-term studies in both preclinical and clinical contexts.

While LDPAM shows promise in evaluating liver fibrosis, several limitations exist. The study had a small sample size with few murine models. Although results are positive, further validation in larger populations and real-world clinical settings is necessary [32]. Secondly, CDOD thresholds for liver fibrosis assessment were based on histopathological analysis using Sirius-red staining, a common but variable and subjective method for visualizing collagen fibers [33]. Future research should explore new methods to validate CDOD thresholds for more reliable fibrosis diagnosis. While LDPAM offers continuous monitoring and deep tissue imaging, its penetration may be limited in obese individuals [34]. Enhancing imaging technology and optimizing parameters have the potential to broaden the applicability of LDPAM to a wider patient demographic. The liver fibrosis model was induced via a 20 % carbon tetrachloride injection, which accelerates fibrosis development and may constrain the generalizability of our findings to some extent. Future research should employ less aggressive models to facilitate a more comprehensive understanding of fibrosis progression over time. Existing literature indicates that fibrosis is not uniformly distributed and that its progression may vary depending on the specific location within the liver [35]. In subsequent investigations, we aim to examine the patterns of fibrosis changes at varying depths within the

liver and to explore the differences among various liver lobes to evaluate the spatial heterogeneity of fibrosis. In this study, we investigated the influence of penetration depth and blood background on the polarization state of light [36]. Our experiments on penetration depth indicate that the polarization state remains stable in the presence of blood tissue up to a depth of 0.7 mm. Beyond this threshold, there is a remarkable decrease in transmitted light intensity, accompanied by a degradation of the polarization state. Furthermore, the phantom experiments demonstrate that LDPAM is capable of effectively imaging collagen fibers despite a strong blood background.

In summary, this research underscores the potential of LDPAM as a valuable non-invasive modality for the diagnosis and monitoring of liver fibrosis. To substantiate the clinical utility of LDPAM in evaluating liver fibrosis, further investigations with larger sample sizes are warranted.

5. Conclusion

This study effectively demonstrated the application of LDPAM as a non-invasive and efficacious tool for assessing liver fibrosis through the quantification of collagen fibers. The CDOD scores facilitate the categorization of liver fibrosis into three distinct stages: normal, early, and advanced. The strong correlation between the CDOD score and the histopathological CPA score, evidenced by a Pearson correlation coefficient of 0.95, underscores LDPAM's accuracy in fibrosis detection. LDPAM emerges as a valuable diagnostic method for visualizing and quantifying collagen deposition. This technique holds considerable promise for enhancing the non-invasive assessment of liver fibrosis, offering a reliable and innovative approach to diagnosing and monitoring this condition.

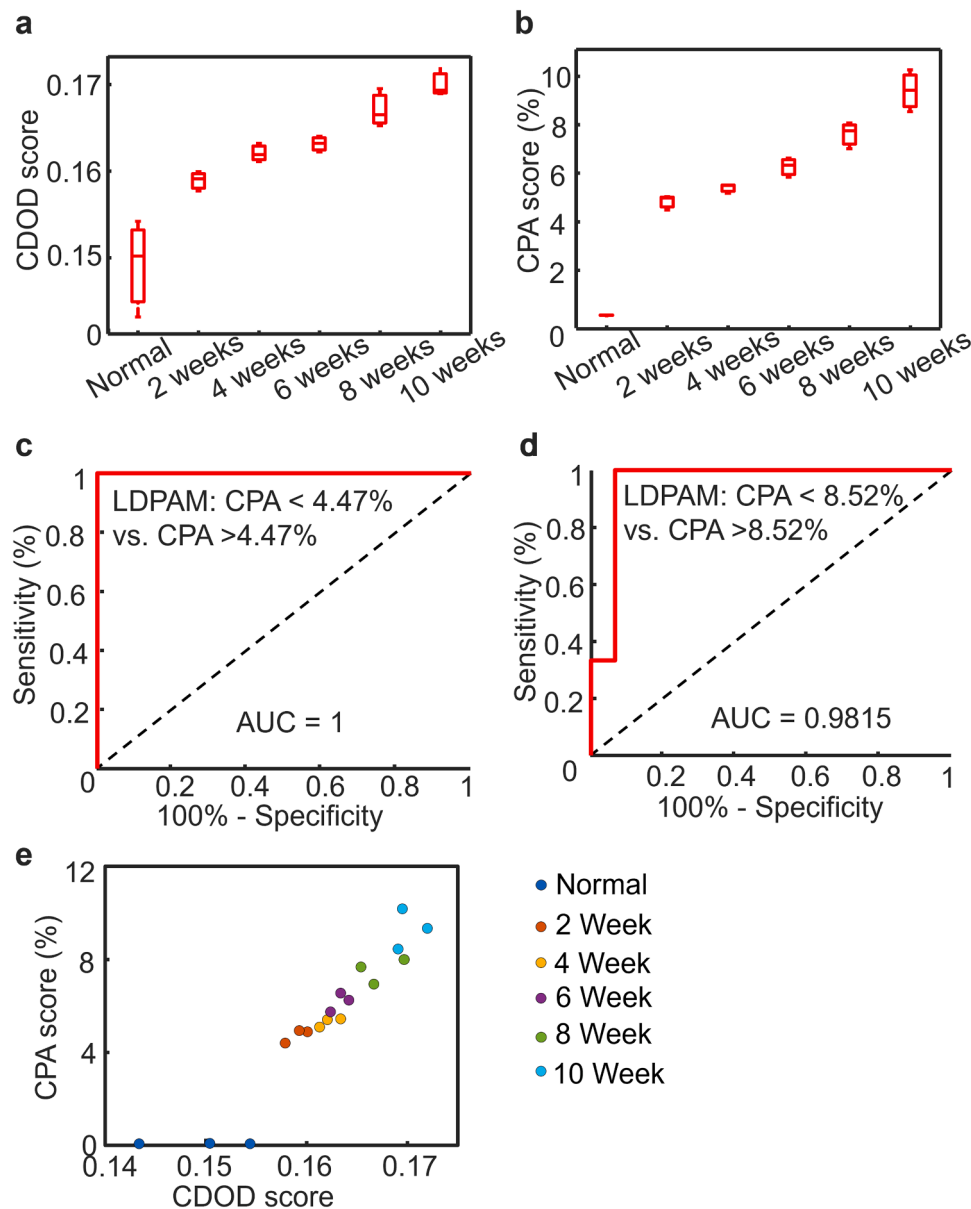


Fig. 8. Quantitative analysis of LDPAM results and correlation analysis with Sirius-red staining results. (a) Results of CDOD score to reflect the content of collagen displayed as a box plots. (b) Results of CPA score in histopathologic analysis. (c) and (d) are receiver operating characteristic analysis of CDOD score to discriminate different liver fibrosis staging by CPA score. (e) Correlation analysis between the CDOD score of the LDPAM and CPA score of the staining results.

Funding

The financial support was partially received from National Natural Science Foundation of China (82402340&82302253), National Key R&D Program of China (2023YFF0715303), GDPH Supporting Fund for Talent Program (KJ01200638) and GDPH Postdoctoral Start-up Funding (BY012022035).

CRediT authorship contribution statement

Yu Kun: Visualization, Methodology, Formal analysis. **Li Honghui:** Writing – original draft, Validation, Methodology, Investigation, Formal analysis, Data curation, Conceptualization. **Qiu Yang:** Writing – original draft, Visualization, Validation, Investigation, Formal analysis, Data curation, Conceptualization. **Zhao Yinghua:** Validation, Writing – review & editing, Conceptualization, Formal analysis, Investigation, Supervision. **Nie Liming:** Supervision, Project administration, Methodology, Funding acquisition, Formal analysis, Conceptualization.

Qi Li: Validation, Methodology. **Chen Jiali:** Validation, Methodology, Formal analysis.

Declaration of Competing Interest

The authors declare that they have no known competing financial interests or personal relationships that could have appeared to influence the work reported in this paper.

Acknowledgments

Y. Qiu and H. Li contributed equally to this work. All authors contributed to the study conception and design. All authors read and approved the manuscript.

Data availability

Data will be made available on request.

References

- [1] E. Tsochatzis, S. Bruno, G. Isgro, A. Hall, E. Theocharidou, P. Manousou, A. P. Dhillon, A.K. Burroughs, T.V. Luong, Collagen proportionate area is superior to other histological methods for sub-classifying cirrhosis and determining prognosis, *J. Hepatol.* 60 (5) (2014) 948–954, <https://doi.org/10.1016/j.jhep.2013.12.023>.
- [2] D. Povero, C. Busletta, E. Novo, L.V. di Bonzo, S. Cannito, C. Paternostro, M. Parola, histopathology, Liver fibrosis: a dynamic and potentially reversible process, *Histol. Histopathol.* 25 (8) (2010) 1075–1091, <https://doi.org/10.14670/HH-25.1075>.
- [3] G. Weijers, I.D. Munsterman, J.M. Thijssen, H. Kuppeveld, J.P. Drenth, E.T. Tjwa, C.L. de Korte, Noninvasive staging of hepatic steatosis using calibrated 2D US with liver biopsy as the reference standard, *Radiology* 306 (3) (2022) e220104, <https://doi.org/10.1148/radiol.220104>.
- [4] L. Alnimer, M. Noureddin, Non-invasive imaging biomarkers for liver steatosis in non-alcoholic fatty liver disease: present and future, *Clin. Mol. Hepatol.* 29 (2) (2023) 394, <https://doi.org/10.3350/cmh.2023.0104>.
- [5] J. Lv, Y. Xu, L. Xu, L. Nie, Quantitative functional evaluation of liver fibrosis in mice with dynamic contrast-enhanced photoacoustic imaging, *Radiology* 300 (1) (2021) 89–97, <https://doi.org/10.1148/radiol.2021204134>.
- [6] S. Zheng, K. He, L. Zhang, M. Li, H. Zhang, P. Gao, Conventional and artificial intelligence-based computed tomography and magnetic resonance imaging quantitative techniques for non-invasive liver fibrosis staging, *Eur. J. Radio.* 165 (2023) 110912, <https://doi.org/10.1016/j.ejrad.2023.110912>.
- [7] J.H. Yu, H.A. Lee, S.U. Kim, Noninvasive imaging biomarkers for liver fibrosis in nonalcoholic fatty liver disease: current and future, *S136-S149*, *Clin. Mol. Hepatol.* 29 (2023), <https://doi.org/10.3350/cmh.2022.0436>.
- [8] J.M. Cormack, Y.-h. Chao, B.T. Archer, K. Kim, K.S. Spratt, M.F. Hamilton, Focused shear wave beam propagation in tissue-mimicking phantoms, *IEEE Trans. Biomed. Eng.* (2023), <https://doi.org/10.1109/TBME.2023.3311688>.
- [9] J.H. Kim, J.H. Yoon, I. Joo, J.M. Lee, Intra-individual comparison of two-dimensional shear wave elastography techniques using plane wave imaging and the multi-beam technique: are they interchangeable in measuring liver fibrosis? *Ultrasonography* 42 (2) (2023) 265, <https://doi.org/10.14366/usg.22135>.
- [10] A. Medyńska-Przećzek, A. Stochel-Gaudyn, A. Wędrychowicz, Liver fibrosis assessment in pediatric population—can ultrasound elastography be an alternative method to liver biopsy? A systematic review, *Adv. Med. Sci.* 69 (1) (2024) 8–20, <https://doi.org/10.1016/j.advms.2023.12.001>.
- [11] L. Petitclercq, G. Gilbert, B.N. Nguyen, A.M. Tang, Liver fibrosis quantification by magnetic resonance imaging, *Top. Magn. Reson Imaging* 26 (6) (2017) 229–241, <https://doi.org/10.1097/RMR.0000000000000149>.
- [12] M. Zerunian, B. Masci, D. Caruso, F. Pucciarelli, M. Polici, S. Nardacci, D. De Santis, E. Iannicelli, A. Laghi, Liver Magnetic Resonance Elastography: Focus on Methodology, Technique, and Feasibility, *Diagnostics* 14 (4) (2024) 379, <https://doi.org/10.3390/diagnostics14040379>.
- [13] T. Lefebvre, C. Wartelle-Bladou, P. Wong, G. Sebastiani, J.-M. Giard, H. Castel, J. Murphy-Lavallée, D. Olivie, A. Ilinca, M.-P. Sylvestre, Prospective comparison of transient, point shear wave, and magnetic resonance elastography for staging liver fibrosis, *Eur. Radio.* 29 (12) (2019) 6477–6488, <https://doi.org/10.1007/s00330-019-06331-4>.
- [14] J. Lv, H. Lan, A. Qin, T. Sun, D. Shao, F. Gao, J. Yao, K. Avnani, L. Nie, Applications, Dynamic synthetic-scanning photoacoustic tracking monitors hepatic and renal clearance pathway of exogenous probes in vivo, *Light Sci. Appl.* 13 (1) (2024) 304, <https://doi.org/10.1038/s41377-024-01644-6>.
- [15] T. Sun, J. Lv, X. Zhao, W. Li, Z. Zhang, L. Nie, In vivo liver function reserve assessments in alcoholic liver disease by scalable photoacoustic imaging, *Photoacoustics* 34 (2023) 100569, <https://doi.org/10.1016/j.pacs.2023.100569>.
- [16] C. Lee, S. Cho, D. Lee, J. Lee, J.-I. Park, H.-J. Kim, S.H. Park, W. Choi, U. Kim, C. Kim, Panoramic volumetric clinical handheld photoacoustic and ultrasound imaging, *Photoacoustics* 31 (2023) 100512, <https://doi.org/10.1016/j.pacs.2023.100512>.
- [17] M.S. Nelson, Y. Liu, H.M. Wilson, B. Li, I.M. Rosado-Mendez, J.D. Rogers, W. F. Block, K.W. Eliceiri, Protocols, Multiscale label-free imaging of fibrillar collagen in the tumor microenvironment, *Methods Mol. Biol.* 2614 (2023) 187–235, https://doi.org/10.1007/978-1-0716-2914-7_13.
- [18] G. Mu, Z. Zhang, D. Cui, W. Chen, Y. Shi, Universal visualization of crystalline orientation for black phosphorus by angle-resolved polarized photoacoustic microscopy, *Opt. Lett.* 48 (10) (2023) 2748–2751, <https://doi.org/10.1364/OL.489709>.
- [19] Z. Zhang, Y. Shi, L. Xiang, D. Xing, Polarized photoacoustic microscopy for vectorial-absorption-based anisotropy detection, *Opt. Lett.* 43 (21) (2018) 5267–5270, <https://doi.org/10.1364/OL.43.005267>.
- [20] Y. Zhou, J. Chen, C. Liu, C. Liu, P. Lai, L. Wang, Single-shot linear dichroism optical-resolution photoacoustic microscopy, *Photoacoustics* 16 (2019) 100148, <https://doi.org/10.1016/j.pacs.2019.100148>.
- [21] W. Qin, H. Li, J. Chen, Y. Qiu, L. Ma, L. Nie, Amphiphilic hemicyanine molecular probes crossing the blood-brain barrier for intracranial optical imaging of glioblastoma, *biomedicine, and art, Sci. Adv.* 11 (3) (2025) eadq5816, <https://doi.org/10.1126/sciadv.adq581>.
- [22] N. Bonod, P. Brianceau, J. Daurios, S. Grosjean, N. Roquin, J.-F. Gleyze, L. Lemaignère, J. Neauport, Linear-to-circular polarization conversion with full-silica meta-optics to reduce nonlinear effects in high-energy lasers, *Nat. Commun.* 14 (1) (2023) 5383, <https://doi.org/10.1038/s41467-023-40709-9>.
- [23] S. Li, B. Zhou, M. Xue, J. Zhu, G. Tong, J. Fan, K. Zhu, Z. Hu, R. Chen, Y. Dong, Macrophage-specific FGF12 promotes liver fibrosis progression in mice, *Hepatology* 77 (3) (2023) 816–833, <https://doi.org/10.1002/hep.32640>.
- [24] J. Berumen, J. Baglieri, T. Kisseleva, K. Mekeel, Liver fibrosis: Pathophysiology and clinical implications, *WIREs Mech. Dis.* 13 (1) (2021) e1499, <https://doi.org/10.1002/wsbm.1499>.
- [25] W. Li, J. Lv, H. Li, L. Song, R. Zhang, X. Zhao, F. Xuan, T. Sun, K. Long, Y. Zhao, L. Nie, Quantification of Vascular Remodeling and Sinusoidal Capillarization to Assess Liver Fibrosis with Photoacoustic Imaging, *Radiology* 314 (1) (2025) e241275, <https://doi.org/10.1148/radiol.241275>.
- [26] A.-Y. Xiu, Q. Ding, Z. Li, C.-Q. Zhang, development, therapy, Doxazosin attenuates liver fibrosis by inhibiting autophagy in hepatic stellate cells via activation of the PI3K/Akt/mTOR signaling pathway, *Drug Des. Dev. Ther.* 15 (2021) 3643–3659, <https://doi.org/10.2147/DDDT.S317701>.
- [27] G.E. Courtoy, I. Leclercq, A. Froidure, G. Schiano, J. Morelle, O. Devuyst, F. Huaux, C. Bouzin, Digital image analysis of picrosirius red staining: A robust method for multi-organ fibrosis quantification and characterization, *Biomolecules* 10 (11) (2020) 1585, <https://doi.org/10.3390/biom10111585>.
- [28] Z. Gong, J. Lin, J. Zheng, L. Wei, L. Liu, Y. Peng, W. Liang, G. Hu, Dahuang zhechong pill attenuates CCl4-induced rat liver fibrosis via the PI3K-Akt signaling pathway, *J. Cell. Biochem.* 121 (2) (2020) 1431–1440, <https://doi.org/10.1002/jcb.29378>.
- [29] T. Luangmonkong, W. Parichatanon, P. Olinga, Targeting collagen homeostasis for the treatment of liver fibrosis: Opportunities and challenges, *Biochem. Pharmacol.* (2023) 115740, <https://doi.org/10.1016/j.bcp.2023.115740>.
- [30] M. Veverka, L. Menozzi, J.J. Mint Yao, devices, The sound of blood: photoacoustic imaging in blood analysis, *Med Nov. Technol. Devices* 18 (2023) 100219, <https://doi.org/10.1016/j.medntd.2023.100219>.
- [31] Z. Zhang, W. Chen, D. Cui, J. Mi, G. Mu, L. Nie, S. Yang, Y. Shi, Collagen fiber anisotropy characterization by polarized photoacoustic imaging for just-in-time quantitative evaluation of burn severity, *Photonics Res.* 11 (5) (2023) 817–828, <https://doi.org/10.1364/PRJ.485022>.
- [32] S. Jeon, J. Kim, D. Lee, J.W. Baik, C. Kim, Review on practical photoacoustic microscopy, *Photoacoustics* 15 (2019) 100141, <https://doi.org/10.1016/j.pacs.2019.100141>.
- [33] A. Arjmand, M.G. Tsipouras, A.T. Tzallas, R. Forlano, P. Manousou, N. Giannakeas, Quantification of liver fibrosis—a comparative study, *Appl. Sci.* 10 (2) (2020) 447, <https://doi.org/10.3390/app10020447>.
- [34] Y. Liu, L. Nie, X. Chen, Photoacoustic molecular imaging: from multiscale biomedical applications towards early-stage theranostics, *Trends Biotechnol.* 34 (5) (2016) 420–433, <https://doi.org/10.1016/j.tibtech.2016.02.001>.
- [35] S. Kurokawa, T. Kobori, M. Yoneda, Y. Ogawa, Y. Honda, T. Kessoku, K. Imajo, S. Saito, A. Nakajima, K.J. Bg Hotta, Identification of differentially methylated regions associated with both liver fibrosis and hepatocellular carcinoma, *BMC Gastroenterol.* 24 (1) (2024) 57, <https://doi.org/10.1186/s12876-024-03149-3>.
- [36] H.-C. Hsu, K.A. Wear, T. Joshua Pfefer, W.C. Vogt, Tissue-mimicking phantoms for performance evaluation of photoacoustic microscopy systems, *Biomed. Opt. Express* 13 (3) (2022) 1357–1373, <https://doi.org/10.1364/BOE.445702>.



Yang Qiu is a master's student at Research Center of Medical Sciences of Guangdong Provincial People's Hospital, Southern Medical University. His research interests primarily focus on developing photoacoustic microscopy systems capable of imaging at greater depths and for medical applications.



Honghui Li is currently a postdoctoral fellow of Research Center of Medical Sciences of Guangdong Provincial People's Hospital, Guangdong Academy of Medical Sciences, Southern Medical University. He got his Ph.D. degree from Xiamen University, China in 2022. His research interests include developing novel biomedical imaging tools based on photoacoustic imaging for preclinical and clinical applications.



Kun Yu is a master's student at the Research Center of Medical Sciences at South China University of Technology. His research interests primarily focus on developing high-speed photoacoustic microscopy systems.



Yinghua Zhao is a chief physician and Ph.D. supervisor at the Department of Medical Imaging of the Third Affiliated Hospital of Southern Medical University, as well as at Southern Medical University. Her laboratory focuses on medical artificial intelligence, with research interests spanning AI-assisted imaging diagnosis, medical image processing, and the development of intelligent diagnostic systems. One of her goals is to advance precision medicine by integrating AI technology into clinical practice, aiming to improve diagnostic accuracy and treatment outcomes.



Jiali Chen obtained her Master's degree in Medical Technology from Southern Medical University in 2022. She is currently pursuing her Ph.D. in Biomedical Engineering at South China University of Technology. Her research focuses on the application of near-infrared II fluorescence and photoacoustic molecular imaging technologies in tumors and metabolism-related diseases.



Liming Nie is a professor and Ph.D. supervisor at Research Center of Medical Sciences of Guangdong Provincial People's Hospital, Guangdong Academy of Medical Sciences, Southern Medical University. His laboratory focuses on optical imaging technology, mainly on photoacoustic microscopy, photoacoustic computed tomography, and other related imaging modalities. One of his aims is to provide effective and low-cost imaging instruments for disease diagnosis and treatment monitoring.



Li Qi received his Ph.D. degree in Optical Engineering in 2016 from Nanjing University. He is currently an associate professor at the Guangdong Provincial Key Laboratory of Medical Image Processing, School of Biomedical Engineering, Southern Medical University in Guangzhou, China. His research interests include photoacoustic imaging and optical coherence tomography.